MJFAS MALAYSIAN JOURNAL OF FUNDAMENTAL AND APPLIED SCIENCES
PRINT ISSN: 2289-5981 | ONLINE ISSN: 2289-599X

RESEARCH ARTICLE

Influence of viscous dissipation on the flow and heat transfer of a Jeffrey fluid towards horizontal circular cylinder with free convection: A numerical study

Syazwani Mohd Zokri [a], Nur Syamilah Arifin [a], Muhammad Khairul Anuar Mohamed [a], Abdul Rahman Mohd Kasim [a], Nurul Farahain Mohammad [b] and Mohd Zuki Salleh [a,*]

[a] Faculty of Industrial Sciences & Technology, Universiti Malaysia Pahang, 26300 Kuantan, Pahang, Malaysia
[b] Department of Computational and Theoretical Sciences, Kulliyyah of Science, International Islamic University Malaysia, 25200 Kuantan, Pahang, Malaysia

* Corresponding author: zuki@ump.edu.my

Article history
Submitted 27 July 2017
Revised 7 October 2017
Accepted 4 January 2018
Published Online 8 Mac 2018

Abstract

This paper focuses on the numerical solution of free convection boundary layer flow past a horizontal circular cylinder in non-Newtonian Jeffrey fluid. The impact of viscous dissipation is discussed. The non-dimensional variables and non-similar transformations are implemented to transform the dimensional partial differential equations into two nonlinear partial differential equations (PDEs). Then, the implicit, unconditionally stable and well-tested Keller-box method is used to solve the PDEs by adding an extra boundary condition at infinity. The impacts of emerging parameters such as ratio of relaxation to retardation times, Deborah number, Prandtl number and Eckert number towards the quantities of physical interest are deliberated through graphical representation. The critical point for Prandtl number and ratio of relaxation to retardation times are investigated to achieve the physically acceptable solutions. It appears from this study that a rise in ratio of relaxation to retardation times tends to boost the velocity profile while declining the temperature profile. The opposite trend of graph is observed for the Deborah number where an increase in Deborah number give rise to decrement in velocity profile but increment in temperature profile. For increasing values of the Eckert number, the skin friction coefficient is found to increase while the Nusselt number is decreased. This study also reveals that for different values of Eckert number, the non-Newtonian Jeffrey fluid pronounces an effective heat transfer rate in comparison to Newtonian fluid.

Keywords: Non-Newtonian Jeffrey fluid, free convection, viscous dissipation effect, horizontal circular cylinder

INTRODUCTION

The action of natural buoyancy forces on the fluid flow is termed as free or natural convection. Principally, the natural buoyancy forces is arising owing to the density gradients in the fluid that is induced by the difference in temperature (Kakac *et al.*, 2013). In recent years, the study of non-Newtonian fluids in free convection has become a topic of interests among researchers. This interest is attributable to the complex nature of fluid used in most engineering applications such as food and polymer processing, cable coating, thermal oil recovery and fossil fuels. In polymer processing, the process of dip coating that involves heat transfer is essential for optimum production of polymer components. Such process is done by dipping the surface to be layered into polymer solution (Middleman, 1977; Roy, 1971).

Of all the non-Newtonian fluid models introduced, the Jeffrey fluid model is selected for the present investigation. This is because, this fluid model can be distinguished among the existing models by its ability of describing both the impact of relaxation and retardation. In fact, this fluid model is fundamentally upgraded from the Maxwell fluid model where the effect of relaxation time can only be described by the Maxwell fluid, but not the retardation times. It is worth mentioning that retardation time refers to the time required by the material to react to deformation. Furthermore, this non-Newtonian fluid can be differentiated with viscous fluid by its nonlinear relationship between shear stress and shear rate. This fluid also exhibits a relatively simple linear model that aids in numerical computation by means of time derivatives in place of convective derivatives. In this manner, the numerical computation is expected to be much easier (Rehman *et al.*, 2015). This fluid model is also established by implementing the Jeffrey fluid term in the momentum equation of the classical Navier stokes (Newtonian) model.

It appears from the literature that the early study on the momentum equation has been done by Blasius (1907). Specifically, he focused on the forced convection boundary layer flow. His study was then continued by Frossling (1958) on the energy equation. Merkin (1976) performed numerical analysis on the free convection boundary layer problem with constant wall temperature. Soon after, Merkin and Pop (1988) tackled the same problem but with boundary condition of constant heat flux. Since then, countless investigations linked to this research field have been conducted. These investigations include the extension of existing mathematical models to different surface geometries, fluids, boundary conditions and the probable engagement of some effects such as magnetohydrodynamic (MHD), viscous dissipation and many more. For example, the micropolar fluid with constant wall temperature has been utilised by Nazar *et al.* (2002). Molla *et al.* (2006; 2009) examined the existence of heat generation with constant wall temperature and constant heat flux, respectively. The problem of natural convection in viscous fluid with Newtonian heating has been solved by Salleh and Nazar (2010). Later, the impact of MHD in nanofluid was studied by Sheikholeslami *et al.* (2012). Kasim *et al.* (2013) studied the viscoelastic fluid past a horizontal circular cylinder with constant heat flux. Prasad *et al.* (2014) considered the presence of suction/injection effect in Jeffrey fluid past a permeable horizontal circular cylinder. Their study revealed that the existence of suction parameter for increasing Deborah number has reduced the skin friction coefficient and Nusselt number. Then, with the purpose of investigating the linear porous media and second-order Forchheimer drag effects, they extended the similar problem in a non-Darcy porous medium (Prasad *et al.*, 2015). More recently, Al-Sharifi *et al.* (2017) scrutinized the model of Jeffrey fluid with the aligned magnetohydrodynamic effect and Newtonian heating boundary condition.

In relation to the existing publications, the primary study of viscous dissipation effect has been attempted by Gebhart (1962). His study suggested that for both cases of isothermal and uniform heat flux, the significant effect of viscous dissipation is observed at the wall of vertical surfaces. Using the same boundary condition, Vajravelu and Hadjinicolaou (1993) revealed that the temperature profile is raised due to the increasing effect of viscous dissipation, which can be measured using the dimensionless parameter, namely Eckert number. Later, Yirga and Shankar (2013) and Azim (2014) examined this effect in an electrically conducting fluid. Mohamed *et al.* (2016a; 2016b) discussed this effect in viscous and nanofluid passing through horizontal circular cylinder. In consideration of Jeffrey fluid, recent examination of this effect was then tackled by Zokri *et al.* (2017) over a stretching sheet. It is found that the prominent viscous dissipation effect is identified in the device that functions at high rotative speed, for example rotating cavities processes.

Therefore, the present study intends to explore the effect of viscous dissipation on the free convection boundary layer flow embedded in Jeffrey fluid past a horizontal circular cylinder. Until now, the authors assured that the present study is yet unpublished by other works.

MATHEMATICAL FORMULATION

The Cauchy stress tensor, $\mathbf{T}$ is the constitutive equation for the model of Jeffrey fluid (Bird *et al.*, 1977)

$$\mathbf{T}=-p\mathbf{I}+\mathbf{S} \quad (1)$$

where

$$\mathbf{S}=\frac{\mu}{1+\lambda}\left(\dot{\gamma}+\lambda_1\ddot{\gamma}\right) \quad (2)$$

Here, $\mathbf{I}$ is the identity tensor, p is the pressure, $\mathbf{S}$ is the extra stress tensor, λ is the ratio of relaxation to retardation times, μ is dynamic viscosity, λ_1 is the retardation time and $\dot{\gamma}$ is the shear rate, where the dot on the quantity represents the time derivatives of the material. Further, both the shear rate and the gradient of shear rate take the following form:

$$\dot{\gamma}=\nabla\mathbf{V}+\left(\nabla\mathbf{V}\right)^T,\ \ddot{\gamma}=\frac{d}{dt}\left(\dot{\gamma}\right) \quad (3)$$

The above equations are introduced to relate the rate of stress and strain fields as well as to represent the behaviors of viscous and elastic of polymer melts that are widely used in polymer processing. In the present attempt, we intend to study the steady free convection boundary layer flow induced by a horizontal circular cylinder embedded in Jeffrey fluid with the impact of viscous dissipation. The physical model of the coordinate system is illustrated in Fig. 1. The $\bar{x}-$ and $\bar{y}-$ coordinates are taken from the lowest point and normal to the sideways of cylinder surface, respectively, with a, T_w and T_∞ representing the radius of circular cylinder, constant and ambient temperature. By incorporating the stress tensor of Jeffrey fluid and viscous dissipation effect in the momentum and energy equations, the following governing equations are obtained (Das *et al.*, 2015; Mohamed *et al.*, 2016a):

$$\frac{\partial\bar{u}}{\partial\bar{x}}+\frac{\partial\bar{v}}{\partial\bar{y}}=0, \quad (4)$$

$$\begin{aligned}\bar{u}\frac{\partial\bar{u}}{\partial\bar{x}}+\bar{v}\frac{\partial\bar{u}}{\partial\bar{y}}&=\frac{\nu}{1+\lambda}\left[\frac{\partial^2\bar{u}}{\partial\bar{y}^2}+\lambda_1\left(\bar{u}\frac{\partial^3\bar{u}}{\partial\bar{x}\partial\bar{y}^2}-\frac{\partial\bar{u}}{\partial\bar{x}}\frac{\partial^2\bar{u}}{\partial\bar{y}^2}+\frac{\partial\bar{u}}{\partial\bar{y}}\frac{\partial^2\bar{u}}{\partial\bar{x}\partial\bar{y}}+\bar{v}\frac{\partial^3\bar{u}}{\partial\bar{y}^3}\right)\right] \quad (5)\\&+g\beta\left(T-T_\infty\right)\sin\left(\frac{\bar{x}}{a}\right),\end{aligned}$$

$$\begin{aligned}\bar{u}\frac{\partial T}{\partial\bar{x}}+\bar{v}\frac{\partial T}{\partial\bar{y}}&=\alpha\frac{\partial^2T}{\partial\bar{y}^2}\\&+\frac{\nu}{C_p(1+\lambda)}\left[\left(\frac{\partial\bar{u}}{\partial\bar{y}}\right)^2+\lambda_1\left(\bar{u}\frac{\partial\bar{u}}{\partial\bar{y}}\frac{\partial^2\bar{u}}{\partial\bar{x}\partial\bar{y}}+\bar{v}\frac{\partial\bar{u}}{\partial\bar{y}}\frac{\partial^2\bar{u}}{\partial\bar{y}^2}\right)\right],\end{aligned} \quad (6)$$

From Eqs. (4) to (6), $\bar{u}$ and $\bar{v}$ are the components of velocity in $\bar{x}$ and $\bar{y}$ directions, where λ represents the ratio of relaxation to retardation times, λ_1 corresponds to the retardation time, α indicates the thermal diffusivity, ν depicts the kinematic viscosity, β signifies the thermal expansion, T implies the local temperature, g is the gravity acceleration and C_p denotes the specific heat capacity at a constant pressure. Noticeably, there exist several mixed derivatives that represent the Jeffrey fluid term arising in Eq. (5). Among them, two derivatives are an order higher than the Newtonian model, for example $\bar{u}\left(\partial^3\bar{u}/\partial\bar{x}\partial\bar{y}^2\right)$ and $\bar{v}\left(\partial^3\bar{u}/\partial\bar{y}^3\right)$. Moreover, the last term of Eq. (6) corresponds to the viscous dissipation effect. Further, the related boundary conditions are

$$\begin{aligned}&\bar{u}(\bar{x},0)=0,\quad \bar{v}(\bar{x},0)=0,\quad T(\bar{x},0)=T_w \quad \text{at} \quad \bar{y}=0\\&\bar{u}(\bar{x},\infty)\to 0,\quad \bar{v}(\bar{x},\infty)\to 0,\quad T(\bar{x},\infty)\to T_\infty \quad \text{as} \quad \bar{y}\to\infty\end{aligned} \quad (7)$$

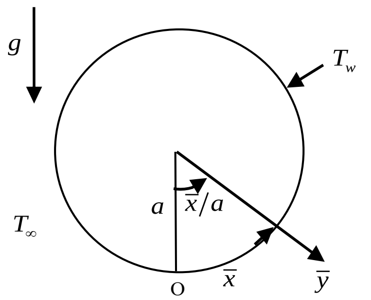

Fig. 1 Geometry of the problem.

The solution is looked via the following governing non-dimensional quantities

$$u=\frac{a}{\nu}Gr^{-1/2}\bar{u},\ v=\frac{a}{\nu}Gr^{-1/4}\bar{v},\ x=\frac{\bar{x}}{a},\ y=Gr^{1/4}\frac{\bar{y}}{a},\ \theta(\eta)=\frac{T-T_\infty}{T_w-T_\infty} \quad (8)$$

Substituting Eq. (8) into Eqs. (4) to (6), these equations give rise to the succeeding expressions:

$$\frac{\partial u}{\partial x}+\frac{\partial v}{\partial y}=0, \quad (9)$$

$$u\frac{\partial u}{\partial x}+v\frac{\partial u}{\partial y}=\frac{1}{1+\lambda}\left[\frac{\partial^2 u}{\partial y^2}+\lambda_2\left(u\frac{\partial^3 u}{\partial x\partial y^2}-\frac{\partial u}{\partial x}\frac{\partial^2 u}{\partial y^2}+\frac{\partial u}{\partial y}\frac{\partial^2 u}{\partial x\partial y}+v\frac{\partial^3 u}{\partial y^3}\right)\right]+\theta\sin x, \tag{10}$$

$$u\frac{\partial \theta}{\partial x}+v\frac{\partial \theta}{\partial y}=\frac{1}{\Pr}\frac{\partial^2\theta}{\partial y^2}+\frac{Ec}{(1+\lambda)}\left[\left(\frac{\partial u}{\partial y}\right)^2+\lambda_2\left(u\frac{\partial u}{\partial y}\frac{\partial^2 u}{\partial x\partial y}+v\frac{\partial u}{\partial y}\frac{\partial^2 u}{\partial y^2}\right)\right], \tag{11}$$

The associate boundary conditions are:

$$\begin{aligned}&u(x,0)=0,\quad v(x,0)=0,\quad \theta(x,0)=1 \quad \text{at} \quad y=0\\ &u(x,\infty)\to 0,\quad v(x,\infty)\to 0,\quad \theta(x,\infty)\to 0 \quad \text{as} \quad y\to\infty\end{aligned} \tag{12}$$

Eqs. (10) and (11) consist of the following dimensionless numbers:

$$\lambda_2=\frac{\lambda_1 Gr^{1/2}\nu}{a^2}\text{(Deborah number)},\ Gr=\frac{g\beta(T_w-T_\infty)a^3}{\nu^2}\text{(Grashof number)},$$
$$Ec=\frac{\nu^2 Gr}{a^2C_p\left(T_w-T_\infty\right)}\text{(Eckert number) and }\Pr=\frac{\mu}{\alpha\rho}\text{(Prandtl number)}$$

Next, Eqs. (9) to (11) are solved by introducing the following functions:

$$\psi=xf(x,y),\quad \theta=\theta(x,y),\quad u=\frac{\partial\psi}{\partial y}\quad\text{and}\quad v=-\frac{\partial\psi}{\partial x} \tag{13}$$

Now, Eq. (9) is automatically satisfied, while Eqs. (10) to (12) result in the subsequent form:

$$\frac{1}{1+\lambda}f'''-\frac{\lambda_2}{1+\lambda}\left[ff^{(iv)}-\left(f''\right)^2\right]+ff''-\left(f'\right)^2+\frac{\sin x}{x}\theta= x\left[f'\frac{\partial f'}{\partial x}-f''\frac{\partial f}{\partial x}-\frac{\lambda_2}{1+\lambda}\left(f'\frac{\partial f'''}{\partial x}-f'''\frac{\partial f'}{\partial x}+f''\frac{\partial f''}{\partial x}-f^{iv}\frac{\partial f}{\partial x}\right)\right] \tag{14}$$

$$\frac{\theta''}{\Pr}+f\theta'=x\left[f'\frac{\partial\theta}{\partial x}-\theta'\frac{\partial f}{\partial x}-x\frac{Ec}{(1+\lambda)}\left(\left(f''\right)^2+\lambda_2\left(xff''\frac{\partial f''}{\partial x}-ff'f'''-x\frac{\partial f}{\partial x}f'f'''+f'\left(f''\right)^2\right)\right)\right] \tag{15}$$

subject to the boundary conditions

$$\begin{aligned}&f(x,0)=0,\quad f'(x,0)=0,\quad \theta(x,0)=1 \quad \text{at} \quad y=0\\ &f'(x,\infty)\to 0,\quad f''(x,\infty)\to 0,\quad \theta(x,\infty)\to 0 \quad \text{as} \quad y\to\infty\end{aligned} \tag{16}$$

In the above equations, f' implies the differentation with respect to the variable y. It is also crucial to remark that Eqs. (14) and (15) are reduced into ordinary differential equations at the lower stagnation point of the cylinder, $x\approx 0$:

$$\frac{1}{1+\lambda}f'''-\frac{\lambda_2}{1+\lambda}\left[ff^{(iv)}-\left(f''\right)^2\right]+ff''-\left(f'\right)^2+\theta=0, \tag{17}$$

$$\frac{1}{\Pr}\theta''+f\theta'=0, \tag{18}$$

with the boundary conditions

$$\begin{aligned}&f(0)=0,\quad f'(0)=0,\quad \theta(0)=1\\ &f'(\infty)\to 0,\quad f''(\infty)\to 0,\quad \theta(\infty)\to 0\end{aligned} \tag{19}$$

Notice that at $x=0$, the Eckert number, Ec is eliminated. Thus, it is considered that the viscous dissipation does not impose any influence at the stagnation region of the cylinder. Next, the skin friction coefficient C_f and the local Nusselt number Nu_x can be written as follows (Molla *et al.*, 2006):

$$C_f=\frac{\tau_w}{\rho U_\infty^2},\quad Nu_x=\frac{aq_w}{k\left(T_w-T_\infty\right)} \tag{20}$$

where $\tau_w=\frac{\mu}{1+\lambda}\left[\frac{\partial\bar{u}}{\partial\bar{y}}+\lambda_1\left(\bar{u}\frac{\partial^2\bar{u}}{\partial\bar{x}\partial\bar{y}}+\bar{v}\frac{\partial^2\bar{u}}{\partial\bar{y}^2}\right)\right]_{\bar{y}=0}$ (Das *et al.*, 2015) and $q_w=-k\left(\frac{\partial T}{\partial\bar{y}}\right)_{\bar{y}=0}$ imply the surface shear stress and heat flux, respectively while k indicates the thermal conductivity. Using Eqs. (13) and (20), the reduced skin friction, $C_fGr^{1/4}$ and reduced Nusselt number, $Nu_xGr^{-1/4}$ are:

$$C_fGr^{1/4}=\frac{1}{1+\lambda}\left[\begin{array}{l}xf''(x,0)\\ +\lambda_2\left\{\begin{array}{l}x^2f'(x,0)\dfrac{\partial f''(x,0)}{\partial x}-x^2f'''(x,0)\dfrac{\partial f(x,0)}{\partial x}\\ +xf'(x,0)f''(x,0)-xf(x,0)f'''(x,0)\end{array}\right\}\end{array}\right]$$

and

$$Nu_xGr^{-1/4}=-\theta'(x,0) \tag{21}$$

RESULTS AND DISCUSSION

Eqs. (14) and (15) along with the boundary conditions (16) are considered to obtain the numerical solutions. However, these equations are difficult to solve analytically due to their complexity and the highly nonlinear equations arising in the momentum and energy equations. Yet, a well-tested and unconditionally stable numerical approach, namely the Keller-box method has been used to generate the numerical results. Detail explanations of these steps can be found in the book written by Na (1980) and Cebeci and Bradshaw (1988).

A comparative study has been done on the variations of $C_fGr^{1/4}$ and $Nu_xGr^{-1/4}$ against x as tabulated in Tables 1 and 2, respectively. A great consistency of the present study with existing publications is achieved; thus, the present codes are assured to be used for obtaining numerical solutions. The numerical results are presented through graphs (Figs. 3 to 20) for several parameters, such as Deborah number λ_2, ratio of relaxation to retardation times λ, Eckert number Ec and Prandtl number $\Pr$, for which they are fixed as $\lambda=0.1$, $\lambda_2=0.1$, $\Pr=0.71$ and $Ec=0.1$, except otherwise declared. The following step size and boundary layer thickness are considered, i.e. $\Delta x=0.01$ and $\Delta y=0.02$ and $y_\infty=8$.

The profiles for velocity $f'(y)$ and temperature $\theta(y)$ are portrayed in Figs. 3 to 8 for different values of λ, λ_2 and $\Pr$. In Figs. 3 and 4, the $f'(y)$ and $\theta(y)$ are sketched to investigate the effect of parameter λ. Initially, a rise in λ is noticed to boost the velocity profile; however, the velocity profile starts to decay to some extent near the freestream. An opposite trend is found in Fig. 4, where $\theta(y)$ is inconsiderably reduced as λ increases. Physically, λ is dependent on the retardation time. An increase in λ signifies weaker retardation time while a decrease in λ indicates stronger retardation time. Such change in retardation time leads to the increment and decrement in the respective momentum and thermal boundary layer thickness.

The influence of λ_2 on the velocity and temperature distributions are drawn in Figs. 5 and 6. In Fig. 5, as λ_2 increases, the intense reduction has been perceived on the velocity component. In essence, the viscoelasticity of material is presented by parameter λ_2, where it is actually combination of both viscous and elastic characteristics that will undergo deformation once the stress is applied. Due to this characteristic, either viscosity or elasticity increases, the velocity of fluid will always reduce. As such, a decrease in velocity profile is predicted (Hayat *et al.*, 2011; Zin *et al.*, 2017). Further, the insignificant effect of λ_2 has been observed at the surface $(y = 0)$; yet, the effect of λ_2 is remarked at midway distance from the surface. Oppositely, a slight increase in temperature profile is seen in Fig. 6 along with the continuous degeneration of profile towards the freestream. It is essential to remark that the present trend of graphs attained are similar with documented result by Prasad *et al.* (2014).

In Figs. 7 and 8, both the velocity and temperature profiles are considerably depreciated for the increasing $\Pr$, which in turn lead to the deterioration of momentum and thermal boundary layer thickness. At the midway distance from the surface of cylinder, it is visibly clear that both profiles encounter significant variations. Furthermore, in comparison to the small $\Pr$, the thermal boundary layer for larger $\Pr$ is thinner. This is because, the thermal diffusivity is relatively lower for larger $\Pr$, hence this results in the reduction of temperature profile.

Figs. 9 and 10 are plotted to identify the critical point for the Prandtl number $\Pr$ and ratio of relaxation to retardation times λ, with the purpose of achieving physically acceptable solution. The impact of λ and $\Pr$ on the $Nu_x Gr^{-1/4}$ at stagnation point, $x = 0$ is illustrated in Fig. 9. It is observed that as $\Pr$ approaches the critical values, $\Pr_c$ a strong increment of heat transfer rate is detected. Furthermore, as λ gets larger, the $\Pr_c$ becomes smaller. For $\lambda = 0.1,\ 1.0$ and 5.0, the critical points are $\Pr_c = 1.1666,\ 04641$ and 0.2397, respectively. Thus, this graph suggests that a physically agreeable solution can be accomplished when $\Pr$ is lower than $\Pr_c$, when subjected to different λ. Meanwhile, the effect of λ_2 and λ on the $Nu_x Gr^{-1/4}$ is shown in Fig. 10, where the acceptable physical solution of λ is highly dependent on the λ_2. The critical points obtained are $\lambda_c = 0.3801,\ 0.7580$ and 2.1386 for the respective values of $\lambda_2 = 0.1,\ 1.0$ and 5.0, which means the higher values of λ_2 constitute to the larger values of the critical point, λ_c.

The variations of $C_f Gr^{1/4}$ and $Nu_x Gr^{-1/4}$ towards different value of $\Pr$ and Ec are plotted in Figs. 11 to 14. It is perceived that the $C_f Gr^{1/4}$ is decreasing due to the increasing value of $\Pr$ as depicted in Fig. 11. This is because, the fluid is more viscous for a larger $\Pr$ and highly viscous fluid will oppose the fluid flow while at the same time lessening the shear stress. On the other hand, Fig. 12 reveals that the $Nu_x Gr^{-1/4}$ has increased and this is attributable to the increase in $\Pr$, thus sequentially enhancing the distribution of heat transfer in the fluid. From Fig. 13, the graph of $C_f Gr^{1/4}$ at the lower stagnation point is observably unique for dissimilar value of Ec. Even so, a slight influence of Ec is spotted far from the stagnation point. Meanwhile, the impact of Ec is trivial at lower stagnation point as displayed in Fig. 14. Nonetheless, as x increases, the $Nu_x Gr^{-1/4}$ has started to receive considerable influence from Ec where the $Nu_x Gr^{-1/4}$ is observably diminished as Ec increases. Furthermore, the velocity and temperature distributions of various Ec demonstrated a unique value, thus the existence of Ec is concluded as to not displaying any changes. Mathematically, this outcome happens because of the termination of Ec at $x = 0$. A study documented by Mohamed *et al.* (2016b) has emphasised the similar result.

Table 1 Comparative values of $C_f Gr^{1/4}$ for different values of x when $\lambda = 0,\ \lambda_2 \to 0$ (very small), $Ec = 0$ and $\Pr = 1$.

	$C_f Gr^{1/4}$					
x	**Merkin (1976)**	**Nazar *et al.* (2002)**	**Molla *et al.* (2006)**	**Azim (2014)**	**Mohamed *et al.* (2016a)**	**Present**
0	0.0000	0.0000	0.0000	0.0000	0.0000	0.0000
$\frac{\pi}{6}$	0.4151	0.4148	0.4145	0.4139	0.4121	0.4120
$\frac{\pi}{3}$	0.7558	0.7542	0.7539	0.7528	0.7538	0.7507
$\frac{\pi}{2}$	0.9579	0.9545	0.9541	0.9526	0.9563	0.9554
$\frac{2\pi}{3}$	0.9756	0.9698	0.9696	0.9678	0.9743	0.9728
$\frac{5\pi}{6}$	0.7822	0.7740	0.7739	0.7718	0.7813	0.7761
π	0.3391	0.3265	0.3264	0.3239	0.3371	0.3302

Table 2 Comparative values of $Nu_x Gr^{-1/4}$ for different values of x when $\lambda = 0,\ \lambda_2 \to 0$ (very small), $Ec = 0$ and $\Pr = 1$.

	$Nu_x Gr^{-1/4}$					
x	**Merkin (1976)**	**Nazar *et al.* (2002)**	**Molla *et al.* (2006)**	**Azim (2014)**	**Mohamed *et al.* (2016a)**	**Present**
0	0.4214	0.4214	0.4214	0.4216	0.4214	0.4214
$\frac{\pi}{6}$	0.4161	0.4161	0.4161	0.4163	0.4163	0.4162
$\frac{\pi}{3}$	0.4007	0.4005	0.4005	0.4006	0.4008	0.4009
$\frac{\pi}{2}$	0.3745	0.3741	0.3740	0.3742	0.3744	0.3743
$\frac{2\pi}{3}$	0.3364	0.3355	0.3355	0.3356	0.3364	0.3363
$\frac{5\pi}{6}$	0.2825	0.2811	0.2812	0.2811	0.2824	0.2814
π	0.1945	0.1916	0.1917	0.1912	0.1939	0.1932

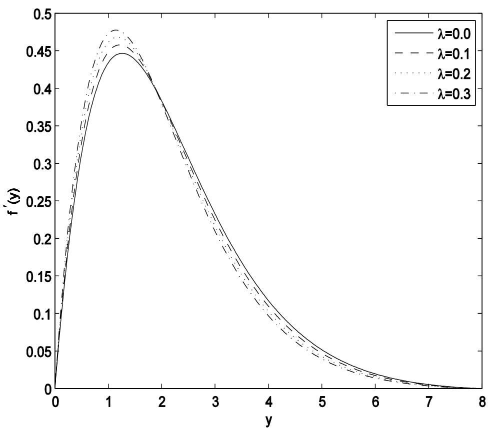

Fig. 3 Impact of λ on $f'(y)$.

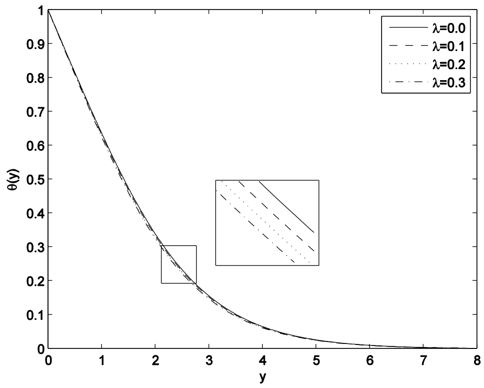

Fig. 4 Impact of λ on $\theta(y)$.

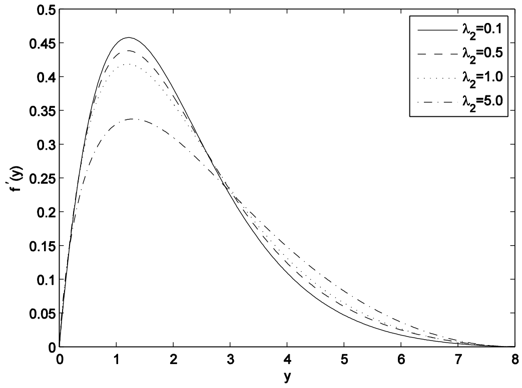

Fig. 5 Impact of λ_2 on $f'(y)$.

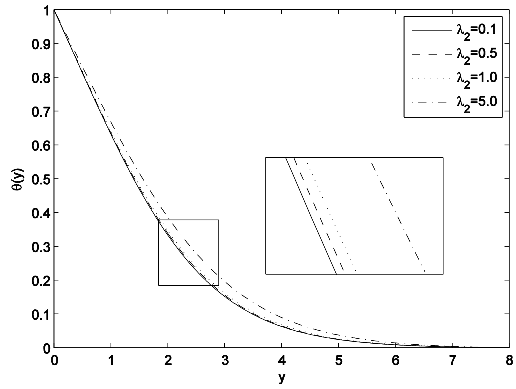

Fig. 6 Impact of λ_2 on $\theta(y)$.

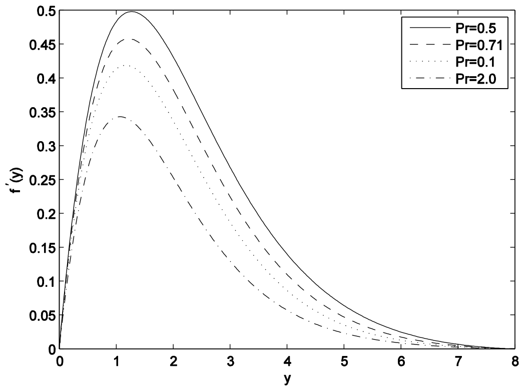

Fig. 7 Impact of Pr on $f'(y)$.

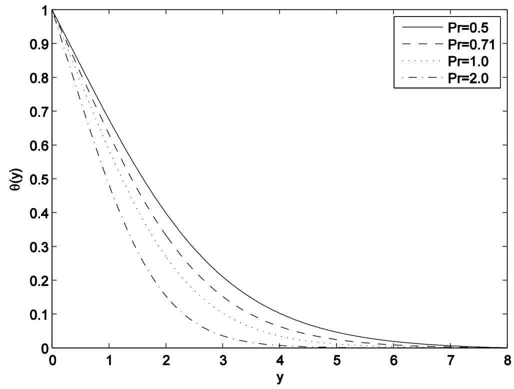

Fig. 8 Impact of Pr on $\theta(y)$.

The impacts of both Pr and Ec on the variations of $C_f Gr^{1/4}$ and $Nu_x Gr^{-1/4}$ are illustrated in Figs. 15 and 16. From Fig. 15, it is seen that the increment of $C_f Gr^{1/4}$ is greater for $\mathrm{Pr} = 0.71$ as compared to $\mathrm{Pr} = 7$ when $Ec = 0.1$ and 0.5. In contrast, Fig. 16 exhibits the opposite trend of the graph, wherein the $Nu_x Gr^{-1/4}$ is increased significantly as a result of the increasing Pr. Correspondingly, higher value of Pr, i.e. $\mathrm{Pr} = 7$ induces the betterment of heat transfer rate, owing to huge kinetic energy offered from bigger Pr.

Figs. 17 and 18 demonstrate the impact of different Pr and λ_2 on $C_f Gr^{1/4}$ and $Nu_x Gr^{-1/4}$ at two different positions of x. Clearly, with an increase in Pr, the value of $C_f Gr^{1/4}$ in Fig. 17 is decreasing at $x = \pi/6$. At $x = 0$, it is found that the graph of $C_f Gr^{1/4}$ does not exist. Further, as Pr increases, the graph plotted in Fig. 18 depicts the increasing value of $Nu_x Gr^{-1/4}$ both at $x = 0$ and $\pi/6$. It is noteworthy from the figure that the effective heat transfer rate occurs at $x = 0$.

The effects of Newtonian and non-Newtonian Jeffrey fluid for increasing value of Ec on $C_f Gr^{1/4}$ and $Nu_x Gr^{-1/4}$ are examined in Figs. 19 and 20. From Fig. 19, the values of $C_f Gr^{1/4}$ for Newtonian fluid is higher in comparison to the non-Newtonian Jeffrey fluid. Meanwhile, Fig. 20 is contradictory to Fig. 19 where the values of $Nu_x Gr^{-1/4}$ for the non-Newtonian Jeffrey fluid are dominant, indicative of the most effectual cooling and heating processes.

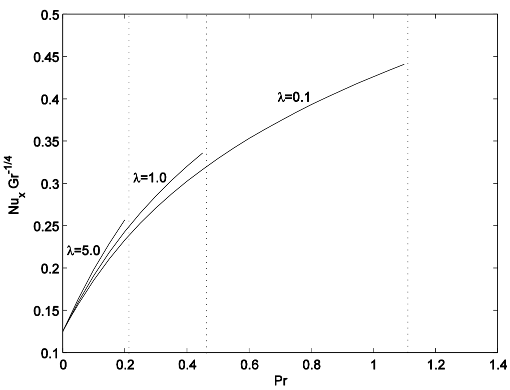

Fig. 9 Variations of $Nu_x Gr^{-1/4}$ for several values of λ and Pr at $x = 0$.

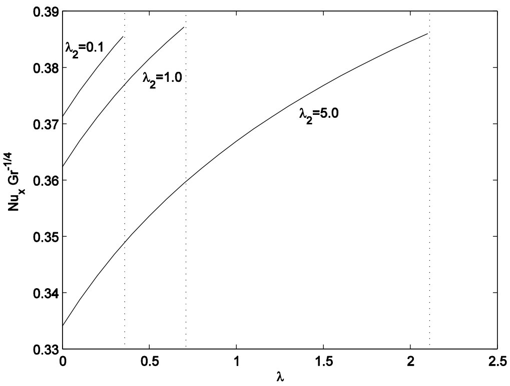

Fig. 10 Variations of $Nu_x Gr^{-1/4}$ for several values of λ_2 and λ at $x = 0$.

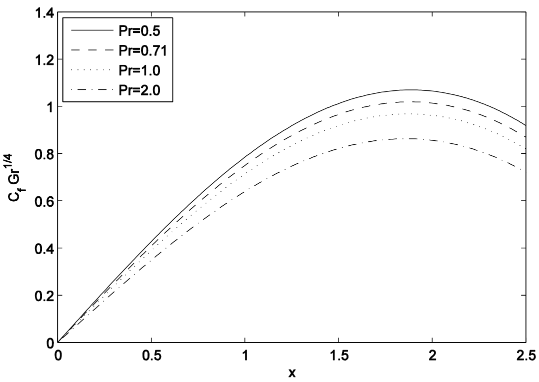

Fig. 11 Variations of $C_f Gr^{1/4}$ for several values of Pr.

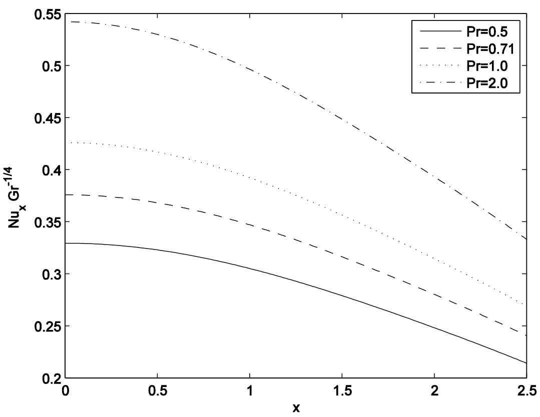

Fig. 12 Variations of $Nu_x Gr^{-1/4}$ for several values of Pr.

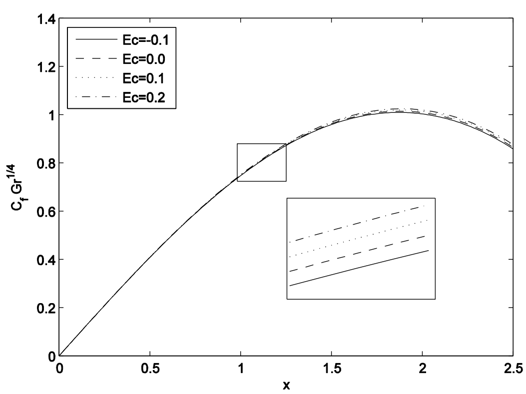

Fig. 13 Variations of $C_f Gr^{1/4}$ for several values of Ec.

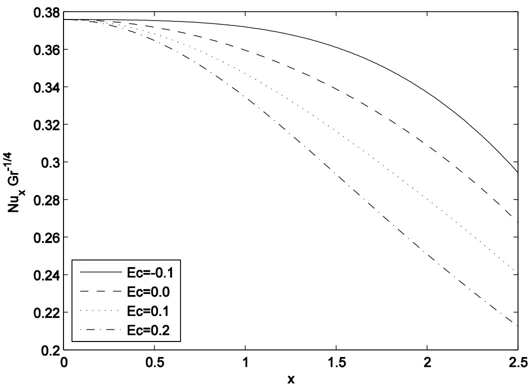

Fig. 14 Variations of $Nu_x Gr^{-1/4}$ for several values of Ec.

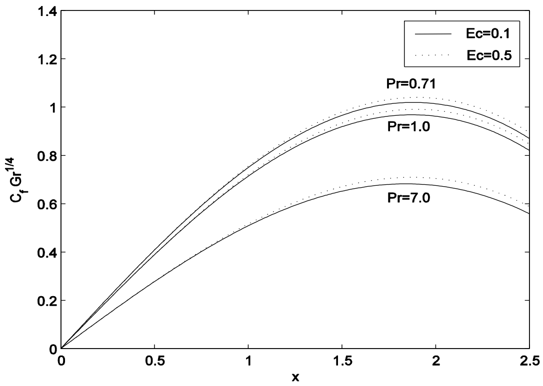

Fig. 15 Variations of $C_f Gr^{1/4}$ for several values of Pr and Ec.

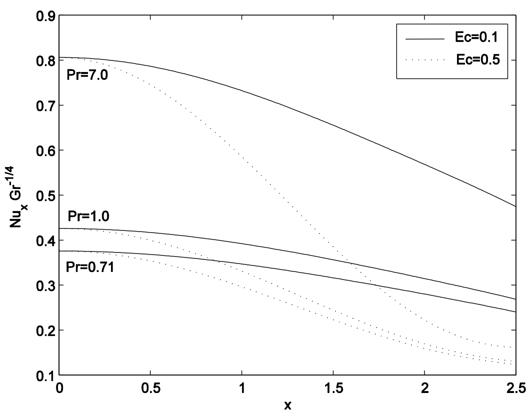

Fig. 16 Variations of $Nu_x Gr^{-1/4}$ for several values of Pr and Ec.

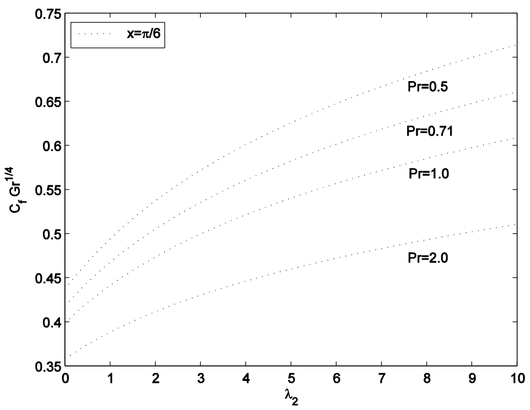

Fig. 17 Variations of $C_f Gr^{1/4}$ for several values of Pr and λ_2.

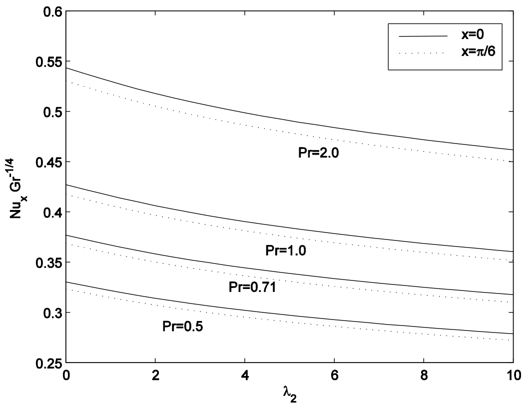

Fig. 18 Variations of $Nu_x Gr^{-1/4}$ for several values of $\Pr$ and λ_2.

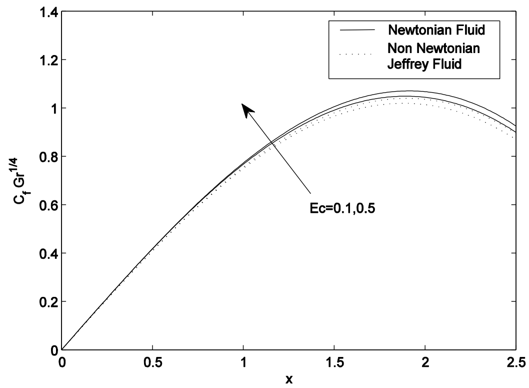

Fig. 19 Variations of $C_f Gr^{1/4}$ for several values of Ec on Newtonian and non-Newtonian Jeffrey fluid.

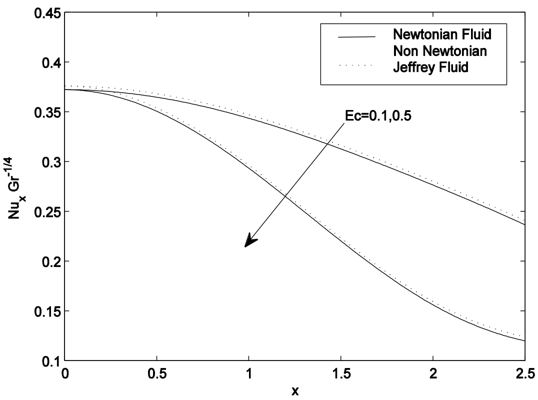

Fig. 20 Variations of $Nu_x Gr^{-1/4}$ for several values of Ec on Newtonian and non-Newtonian Jeffrey fluid.

CONCLUSION

The important findings of this study can be concluded as follows:

- The values of $\Pr$ are significantly dependent on λ at the lower stagnation point of the cylinder.
- The values of λ are strongly dependent on λ_2 at the lower stagnation point of the cylinder.
- Increasing the value of $\Pr$ will decrease the $f'(y)$, $\theta(y)$ and $C_f Gr^{1/4}$ while increasing the $Nu_x Gr^{-1/4}$.
- The $C_f Gr^{1/4}$ rises with the rising value of Ec while declining for rising value of $\Pr$.
- For increasing values of both $\Pr$ and Ec, the $Nu_x Gr^{-1/4}$ is strongly decreased.
- For increasing $\Pr$ and λ_2, the graph of $C_f Gr^{1/4}$ does not exist at $x=0$, while at $x=\pi/6$, the $C_f Gr^{1/4}$ is noticeably decreased.
- For increasing $\Pr$ and λ_2, the $Nu_x Gr^{-1/4}$ is increased. However, the increase in $Nu_x Gr^{-1/4}$ is pronounced at $x=0$ rather than $x=\pi/6$.
- For increasing Ec, the rate of heat transfer of non-Newtonian Jeffrey fluid is more effective than Newtonian fluid.

ACKNOWLEDGEMENT

This study is fully funded by research grants (RDU170358, PGRS1703100 and RDU160330) received from the Universiti Malaysia Pahang. The authors are gratefully acknowledged the financial support.

REFERENCES

Al-Sharifi, H., Kasim, A., Aziz, L., Salleh, M., and Shafie, S. (2017). Influence of aligned magnetohydrodynamic of Jeffrey fluid across a stretching sheet. *Indian Journal of Science and Technology, 10*(7), 1-5.

Azim, N. (2014). Effects of viscous dissipation and heat generation on MHD conjugate free convection flow from an isothermal horizontal circular cylinder. *SOP Transactions on Applied Physics, 1*(3), 1-11.

Bird, R. B., Armstrong, R. C., Hassager, O., and Curtiss, C. F. (1977). *Dynamics of Polymeric Liquids* (Vol. 1). New York: Wiley.

Blasius, H. (1907). *Grenzschichten in Flüssigkeiten mit kleiner Reibung*. Leipzig, Saxony, Germany: Druck von BG Teubner.

Cebeci, T., and Bradshaw, P. (1988). *Physical and Computational Aspects of Convective Heat Transfer*. New York: Springer.

Das, K., Acharya, N., and Kundu, P. K. (2015). Radiative flow of MHD Jeffrey fluid past a stretching sheet with surface slip and melting heat transfer. *Alexandria Engineering Journal, 54*(4), 815-821.

Frossling, N. (1958). Calculation by series expansion of the heat transfer in laminar, constant-property boundary layers at nonisothermal surfaces. *Arkiv Fysik, 14*, 143.

Gebhart, B. (1962). Effects of viscous dissipation in natural convection. *Journal of Fluid Mechanics, 14*(02), 225-232.

Hayat, T., Awais, M., Asghar, S., and Hendi, A. A. (2011). Analytic solution for the magnetohydrodynamic rotating flow of Jeffrey fluid in a channel. *Journal of Fluids Engineering, 133*(6), 061201-061207.

Kakac, S., Yener, Y., and Pramuanjaroenkij, A. (2013). *Convective Heat Transfer*. Boca Raton, Forida, United States: CRC Press.

Kasim, A. R. M., Mohammad, N. F., Shafie, S., and Pop, I. (2013). Constant heat flux solution for mixed convection boundary layer Viscoelastic fluid. *Heat and Mass Transfer, 49*(2), 163-171.

Merkin, J., and Pop, I. (1988). A note on the free convection boundary layer on a horizontal circular cylinder with constant heat flux. *Wärme-und Stoffübertragung, 22*(1-2), 79-81.

Merkin, J. H. (1976). Free convection boundary layer on an isothermal horizontal cylinder. *American Society of Mechanical Engineers and American Institute of Chemical Engineers, Heat Transfer Conference*. 9-11 August 1976. St. Louis, USA, 1-4.

Middleman, S. (1977). *Fundamentals of Polymer Processing*. New York: McGraw-Hill.

Mohamed, M. K. A., Noar, N. A. Z. M., Salleh, M. Z., and Ishak, A. (2016a). Free convection boundary layer flow on a horizontal circular cylinder in a nanofluid with viscous dissipation. *Sains Malaysiana, 45*(2), 289-296.

Mohamed, M. K. A., Sarif, N. M., Kasim, A. R. M., Noar, N. A. Z. M., Salleh, M. Z., and Ishak, A. (2016b). Effects of viscous dissipation on free convection boundary layer flow towards a horizontal circular cylinder. *ARPN Journal of Engineering and Applied Sciences, 11*(11), 7258-7263.

Molla, M. M., Hossain, M. A., and Paul, M. C. (2006). Natural convection flow from an isothermal horizontal circular cylinder in presence of heat generation. *International Journal of Engineering Science, 44*(13–14), 949-958.

Molla, M. M., Paul, S. C., and Hossain, M. A. (2009). Natural convection flow from a horizontal circular cylinder with uniform heat flux in presence of heat generation. *Applied Mathematical Modelling, 33*(7), 3226-3236.

Na, T. Y. (1980). *Computational Methods in Engineering Boundary Value Problems* (Vol. 145). New York: Academic Press.

Nazar, R., Amin, N., and Pop, I. (2002). Free convection boundary layer on an isothermal horizontal circular cylinder in a micropolar fluid. *Heat Transfer, 2*, 525-530.

Prasad, V. R., Gaffar, S. A., Reddy, E. K., and Bég, O. A. (2014). Flow and heat transfer of Jeffreys non-Newtonian fluid from horizontal circular cylinder. *Journal of Thermophysics and Heat Transfer, 28*(4), 764-770.

Prasad, V. R., Gaffar, S. A., Reddy, E. K., and Bég, O. A. (2015). Numerical study of non-Newtonian Jeffreys fluid from a permeable horizontal isothermal cylinder in non-Darcy porous medium. *Journal of the Brazilian Society of Mechanical Sciences and Engineering, 37*(6), 1765-1783.

Rehman, M., Noreen, S., Haider, A., and Azam, H. (2015). Effect of heat sink/source on peristaltic flow of Jeffrey fluid through a symmetric channel. *Alexandria Engineering Journal, 54*(3), 733-743.

Roy, S. C. (1971). Withdrawal of cylinders from non-Newtonian fluids. *The Canadian Journal of Chemical Engineering, 49*(5), 583-589.

Salleh, M. Z., and Nazar, R. (2010). Free convection boundary layer flow over a horizontal circular cylinder with Newtonian heating. *Sains Malaysiana, 39*(4), 671-676.

Sheikholeslami, M., Gorji-Bandpay, M., and Ganji, D. D. (2012). Magnetic field effects on natural convection around a horizontal circular cylinder inside a square enclosure filled with nanofluid. *International Communications in Heat and Mass Transfer, 39*(7), 978-986.

Vajravelu, K., and Hadjinicolaou, A. (1993). Heat transfer in a viscous fluid over a stretching sheet with viscous dissipation and internal heat generation. *International Communications in Heat and Mass Transfer, 20*(3), 417-430.

Yirga, Y., and Shankar, B. (2013). Effects of thermal radiation and viscous dissipation on magnetohydrodynamic stagnation point flow and heat transfer of nanofluid towards a stretching sheet. *Journal of Nanofluids, 2*(4), 283-291.

Zin, N. A. M., Khan, I., and Shafie, S. (2017). Exact and numerical solutions for unsteady heat and mass transfer problem of Jeffrey fluid with MHD and Newtonian heating effects. *Neural Computing and Applications*, 1-17.

Zokri, S. M., Arifin, N. S., Mohamed, M. K. A., Salleh, M. Z., Kasim, A. R. M., and Mohammad, N. F. (2017). Influence of radiation and viscous dissipation on magnetohydrodynamic Jeffrey fluid over a stretching sheet with convective boundary conditions. *Malaysian Journal of Fundamental and Applied Sciences, 13*(3), 279-284.